NANO LETTERS
Letter
Cite This: Nano Lett. 2018, 18, 2365−2372
pubs.acs.org/NanoLett

# Magnetic Iron Oxide Nanowires Formed by Reactive Dewetting

Roger A. Bennett,*[,†] Haitham A. Etman,[†] Hannah Hicks,[†] Leah Richards,[†] Chen Wu,[‡,∥] Martin R. Castell,[‡] Sarnjeet S. Dhesi,[§] and Francesco Maccherozzi[§]

[†]Department of Chemistry, University of Reading, Reading, Berkshire RG6 6AD, United Kingdom
[‡]Department of Materials, University of Oxford, Parks Road, Oxford, OX1 3PH, United Kingdom
[§]Diamond Light Source Ltd, Diamond House, Harwell Science and Innovation Campus, Didcot, Oxfordshire OX11 0DE, United Kingdom

Supporting Information

**ABSTRACT:** The growth and reactive dewetting of ultrathin films of iron oxides supported on Re(0001) surfaces have been imaged in situ in real time. Initial growth forms a nonmagnetic stable FeO (wüstite like) layer in a commensurate network upon which high aspect ratio nanowires of several microns in length but less than 40 nm in width can be fabricated. The nanowires are closely aligned with the substrate crystallography and imaging by X-ray magnetic circular dichroism shows that each contain a single magnetic domain. The driving force for dewetting appears to be the minimization of strain energy of the $Fe_3O_4$ crystallites and follows the Tersoff and Tromp model in which strain is minimized at constant height by extending in one epitaxially matched direction. Such wires are promising in spintronic applications and we predict that the growth will also occur on other hexagonal substrates.

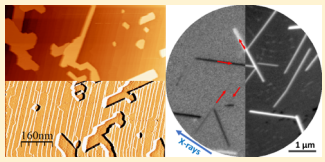


**KEYWORDS:** *$Fe_3O_4$, Re(0001), spintronics, XMCD, STM, XPEEM, LEEM, LEED, oxide ultrathin films*

The continued interest in developing electronic devices in which the electron spin is manipulated to create spin polarized electron currents has generated much fundamental research into materials, their interfaces, grain boundaries, and defects. Of particular importance are the half-metallic ferromagnetic materials in which the electronic density of states should be as near 100% spin polarized at the Fermi level as possible to enable spin polarized transport and the development of magnetoresistance and spin valve type devices. In this class of materials, magnetite ($Fe_3O_4$) has become a leading prospect due to high spin polarization[1] and a Curie temperature of over 800 K.[2] It also displays a metal−insulator Verwey transition at 123 K in which structural distortions lead to charge localization and to the formation of linear Fe ion trimerons.[3,4] The self-organization of the charge and orbital states couples the spin order and magnetism to the Verwey distortion.[3] Both magnetization and structural distortions found in the bulk materials are modified in nanostructures with the Verwey transition suppressed below 20 nm and disappearing at 6 nm-sized nanoparticles.[5]

Controlled synthesis of magnetite nanostructures on surfaces or electrodes is important in the measurement of fundamental material properties and the ongoing development of spintronics.[6,7] Pulsed laser deposition has been demonstrated to grow magnetite nanowires aligned along ⟨110⟩ out of the plane of an $Al_2O_3(0001)$ substrate[8] due to mismatched thermal expansion coefficients between substrate and growing film. Above 873 K, the compressive strain is sufficient to drive out of plane growth of 100 nm diameter nanowires from low-angle grain boundaries between epitaxially grown thick $Fe_3O_4(111)$ oriented films creating a dense nanowire forest. Pyramidal magnetite nanocrystals[9] can be formed by dewetting (at 1373 K) an $Fe_3O_4$ film grown (at 673 K) on $SrTiO_3(001)$ and redepositing $Fe_3O_4$ at high temperature, despite the large lattice mismatch (−7.5%). The substrate orientation stabilizes the growth of a (001) oriented film and the dewetting process leaves (001)-oriented islands that act as seeding centers for the formation of square pyramids with (111) side facets exposed. The nanopyramid structure was reported to reduce the coercive field in comparison to conventional magnetite films, an effect that was dependent upon pyramid size.

On metal substrates wetting layers are far more common due to the larger difference in surface free energies between oxides and metals. Indeed the wetting of metals by oxides is the origin of the strong metal support interaction in catalysis in which surface reactive metal sites are modified, usually blocked, by a thin layer of oxide from the support moving over the metal. First proposed by Tauster in 1978[10] and imaged shortly thereafter by transmission electron microscopy[11,12] in real catalytic materials, the mobility and responsiveness of transition metal oxide materials to their environment has proven to be a cornerstone concept in catalysis. The more recent development of advanced scanning probe microscopies has allowed imaging and identification of these layers on model crystalline systems on a per nanoparticle basis for a number of oxides including $Fe_3O_4$, $TiO_2$, and $SrTiO_3$.[13] Model studies of this effect have led to a plethora of investigations of ultrathin oxides grown on well-defined single crystal metal substrates[14] to further understand the structure and behavior of these important material systems.

**Received:** December 18, 2017
**Revised:** February 26, 2018
**Published:** March 21, 2018



DOI: 10.1021/acs.nanolett.7b05310
Nano Lett. 2018, 18, 2365−2372

In this Letter, we report the formation of magnetic iron oxide nanowires by dewetting from an epitaxial wetting-layer overcoated with Fe in a low oxygen overpressure. The nanowires grow aligned with the crystallographic directions of the substrate forming high aspect ratio straight wires. A thin wetting layer remains on the surface and only the wires show ferro(ferri)magnetism in X-ray magnetic circular dichroism (XMCD) imaging by photoelectron emission microscopy (PEEM). Cross-sectional scanning tunneling microscopy (STM) experiments across the wires show dominant step heights consistent with the magnetite structure.

Full experimental details are given in Supporting Information (SI) and here we give brief comments on the methodology employed to grow, image and analyze the nanostructures. Experiments were performed in two ultrahigh vacuum (UHV) systems, one based on beamline I06 of the Diamond synchrotron for LEEM, PEEM, XMCD, and LEED and the second at the University of Reading for STM, LEED, and XPS. The clean Re(0001) crystal was prepared by cycles of annealing at 1300 K in $O_2$ and flash annealing in UHV to 2300 K following an established method.[15] Iron was deposited in situ by electron beam physical vapor deposition and oxides formed by post deposition annealing at various temperatures and pressures of $O_2$. Formation of nanowires required at least two deposition steps, the first to form an oxide wetting layer and a second thicker Fe overlayer which oxidizes to form the nanowires. The growth conditions and pertinent imaging parameters such as tunneling current ($I_t$) and sample bias ($V_b$) are given in the text and figure captions.

The formation of the first oxide layer was made by evaporation of Fe metal onto the Re(0001) surface maintained at an elevated temperature (510−773 K), followed by oxidation at $1 \times 10^{-7}$ mbar $O_2$. The evaporator flux and completion time for a monolayer (ML, where we define 1 ML as the highest density of Fe that can be grown on Re(0001) before a second layer forms) could be determined by the use of STM[16] (and corresponding XPS and LEED measurements) in the Reading UHV system or by either LEED or direct LEEM imaging in the Diamond UHV system (Movie 1 in SI). Figure 1 shows the evolution of the surface as the Fe monolayer grows on the Re substrate imaged in situ by LEEM at 17.25 eV beam energy. This energy was chosen to highlight the atomic step edges as dark lines, and the approximately triangular Fe islands as dark features against the gray terraces. The LEED pattern from a 1 ML Fe film, Figure 1b, does not display any superstructure spots which indicates that Fe grows pseudomorphically in the first monolayer. The LEED pattern is 6-fold symmetric due to the A-B-A hcp stacking sequence of the substrate[15] presenting both A and B terminations at the surface. The second layer of Fe forms approximately triangular islands rotated 60° with respect to each other on alternating terraces which is also due to these two terminations. The two monolayer thick islands clearly show up brighter in X-ray absorption (XAS) imaging modes, Figure 1c, where the image contrast is formed from the difference between the intensity at the Fe $L_3$ absorption edge and off resonance (pre edge), as would be expected due to the increased X-ray absorption at the Fe $L_3$ edge. The XMCD analysis of such films (not shown) shows no discernible contrast indicating that these ultrathin heteroepitaxial layers are not ferromagnetic.

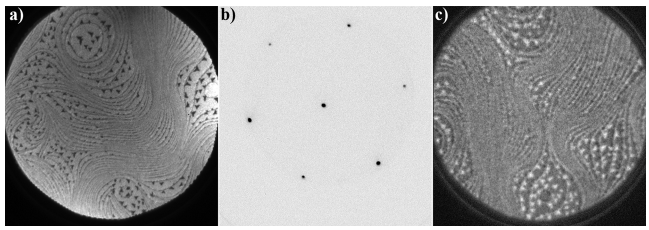


**Figure 1.** Fe deposition on Re(0001) at 500 K while LEEM imaging (17.25 eV, 15 $\mu$m field of view (FOV)). (a) Surface structure at just over 1 ML with crystallographic step edges showing as dark continuous lines and terraces as uniform gray and (b) LEEM-LEED of this surface showing (1 × 1) pattern at 34.85 eV beam energy. (c) An XPEEM XAS intensity image with 15 $\mu$m FOV taken as the difference between signal at $h\nu$ = 707.3 eV on the Fe $L_3$ absorption edge and off resonance (pre-edge) at $h\nu$ = 702 eV.

By heating such a Fe monolayer momentarily to 870 K while it is exposed to $1 \times 10^{-7}$ mbar $O_2$ (and allowing it to cool in the gas), we generate a complete oxide wetting layer in registry with the substrate. A coincidence lattice forms composed of 8 FeO overlayer (3.1 Å) unit cells to 9 Re substrate (2.76 Å) unit cells as shown in Figure 2. The structures seen in the STM are due to a moiré pattern induced by a periodic fit of overlayer structures to the substrate over distances of approximately 2.48 nm with atomic scale features at shorter length scales. Grain boundaries and the change of terrace orientation at step edges give rise to alternative moiré patterns and hence these features can image differently by STM (Figure 2b). LEED patterns for 1 ML oxidized films grown in the Reading STM laboratory (Figure 2c) and in the Diamond I06 PEEM system (Figure 2d) are in very good agreement and show the transferability of growth protocols between the two instruments. XPS indicates that the Re substrate is not oxidized, and we conclude that the

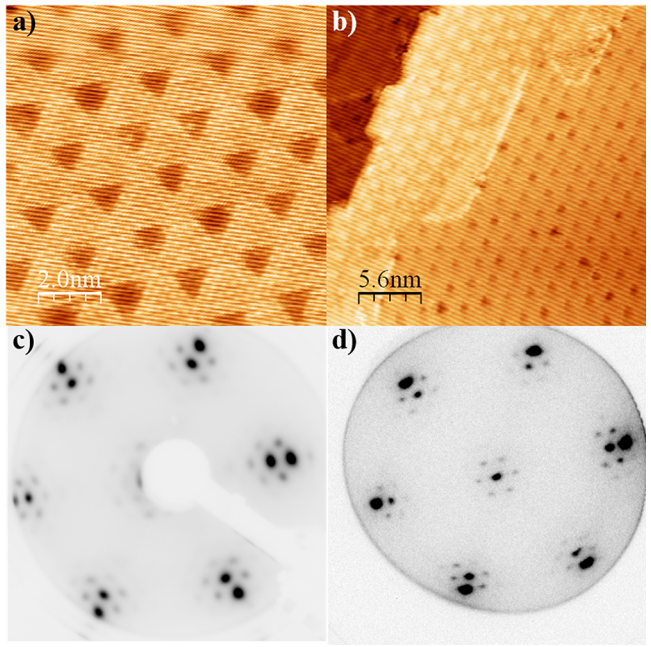


**Figure 2.** (a,b) High-resolution STM images of the FeO monolayer grown on Re(0001) showing periodic Moiré structure due to misfit of the overlayer to the substrate ($I_t$ = 0.2 nA and $V_b$ = 0.1 V). Step edges and grain boundaries between regions of the film change this misfit resulting in various appearances in STM ($I_t$ = 0.5 nA and $V_b$ = 1.5 V). (c) Conventional LEED (60 eV) and (d) microspot LEEM/LEED (54 eV) show near identical patterns from the FeO monolayer.



DOI: 10.1021/acs.nanolett.7b05310
Nano Lett. 2018, 18, 2365−2372

LEED and STM results indicate that this FeO layer is structurally similar to that commonly found on other hexagonal metal substrates, for example on Pt(111)[17,16] or Ru(0001), in which the Fe is on the metal with oxygen terminating to vacuum.[14c,18] XMCD measurements on these films (and those where a second layer of FeO had just begun to grow) show no magnetic structures. We note that 1 ML wüstite films grown on Ru(0001), for which spin polarized LEEM measurements have been reported,[14d] also do not show any magnetism.

To form nanowires, we use this FeO(111) oriented monolayer as a substrate and deposit further Fe and oxidize again. Deposition in UHV of two or more monolayers of iron onto this wetting layer at temperatures between 300 and 373 K leads to the reduction of contrast in the LEED and the appearance of diffraction spots running from the (0,0) spot as the beam energy is varied which is indicative of faceted structures (Movie 4 in SI). The LEEM images at this stage are also reduced in contrast but show no new features and we conclude that very small three dimensional (3D) iron rich islands are formed on the surface which are below the resolution of the LEEM. This result for the growth of Fe on FeO(111) films is similar to that for Fe on $Fe_3O_4$(111) surfaces in which small nanoclusters initially nucleate followed by 3D growth.[19]

However, heating of such Fe/FeO/Re(0001) layered systems in an $O_2$ pressure of $\sim 1 \times 10^{-7}$ mbar while slowly increasing the temperature leads to a remarkable change in surface morphology. First, at ~700 K a dynamic change to the whole surface occurs and is viewed in LEEM as a bright front progressing through the field of view. Such changes in LEEM imaging have recently been noted for mixed Fe oxide films on Pt(111) undergoing various phase transformations,[14b,20] such as compositional changes from $Fe_3O_4$ to $\alpha$-$Fe_2O_3$ (hematite) and for structural only transformations from $\gamma$-$Fe_2O_3$ (maghemite) to $\alpha$-$Fe_2O_3$. These studies were undertaken at higher oxygen pressures (to drive the formation of $Fe_2O_3$) than we use here. We find that the main structural events that occur to create nanowires happen after this reaction front has passed (Movie 2 in SI), and hence we will not comment further on this interesting phenomenon. Upon continued heating to ~770 K, the surface begins to rapidly restructure with terraces changing contrast dramatically in LEEM and with the apparent dewetting and aggregation of islands that grow into the nanowires shown in Figure 3 (and as Movies 2 and 3 in SI). These nanowires are very long (typically up to several micrometers) and narrow (a few tens of nanometers) while crossing many step edges. They also appear to be closely aligned with the crystallography of the substrate and hence run in three dominant directions. On close inspection some wires are seen to have grown 10° away from the principal growth direction and so two orientations are present ±5° from a substrate symmetry direction. It should be noted that without the additional Fe, the FeO(111) on Re(0001) system on its own is stable up to these temperatures and slightly beyond so we conclude that additional Fe is crucial to the nanowire formation.

Figure 3a shows a 10 $\mu$m field of view (FOV) LEEM image at 1.67 eV of these nanowires in which they are seen to extend over several microns in length and across many step edges of the Re(0001) substrate without deviation. The remaining surface has a clearly defined step structure along with some regions between the wires in which the film has not fully dewet (appearing bright in the image). Figure 3b shows the accompanying microspot LEED pattern at 100 eV in which a very well-defined FeO(111) on Re(0001) is the principal component (cf. Figure 2c) along with some running spots arising from faceted structures on the surface. The small size of the nanowires and thermal drift of the sample stage precluded microspot LEED from a single nanowire and so these running spots may arise from inclined surfaces on both the nanowires and the incompletely dewet structures. Figure 3c shows a 6 $\mu$m FOV XAS image in which the intensity is proportional to the total X-ray absorption at the Fe $L_3$ edge (full sequence of frames in Movie 5 in SI). The high intensity nanowires are Fe rich in comparison to the intervening space between islands, however, some faint areas are visible between islands in which incomplete dewetting leaves residual clusters of small islands, in agreement with the LEEM in Figure 3a. The nanowires are therefore much thicker than the wetting layer and the residual islands.

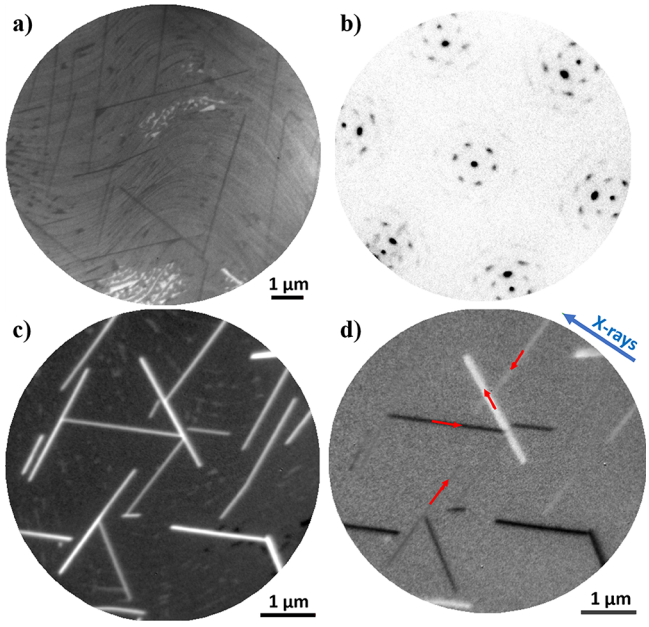


**Figure 3.** Real and reciprocal space images of the dewet nanostructures. Panel a is a 10 $\mu$m FOV LEEM image at 1.67 eV showing nanowires crossing substrate steps with smaller regions of bright and dark islands due to incomplete dewetting. Panel b is a microspot LEED image taken at 100 eV in which the wetting layer pattern is dominant with a superposition of very weak running spots and streaks (due to inclined planes of 3D structures on the surface). Panel c is a 6 $\mu$m FOV image of the XAS signal and identifies the nanowires as Fe rich and hence thick structures. Panel d covers the same 6 $\mu$m FOV as Panel c but with contrast derived from the XMCD signal which indicates that each nanowire displays a single magnetic domain (see text for details, and SI for details on XMCD image formation methodology).

The analysis of the XMCD image of the same area, Figure 3d, suggests that all of the wires are monodomain and are magnetized along their principal axis. The value of the three distinct XMCD intensities that each nanowire may take (black, white, or gray) arises from the dichroism effect being proportional to the cosine of the angle between the photon momentum and the local magnetization and is therefore compatible with the magnetization directions indicated by the red arrows in Figure 3d. Apparent junctions between nanowires visible in Figure 3c are sharp and magnetically well-defined in Figure 3d. The nonmagnetic surface between wires, characterized by zero XMCD signal, may be the result of a complete



DOI: 10.1021/acs.nanolett.7b05310
Nano Lett. 2018, 18, 2365−2372

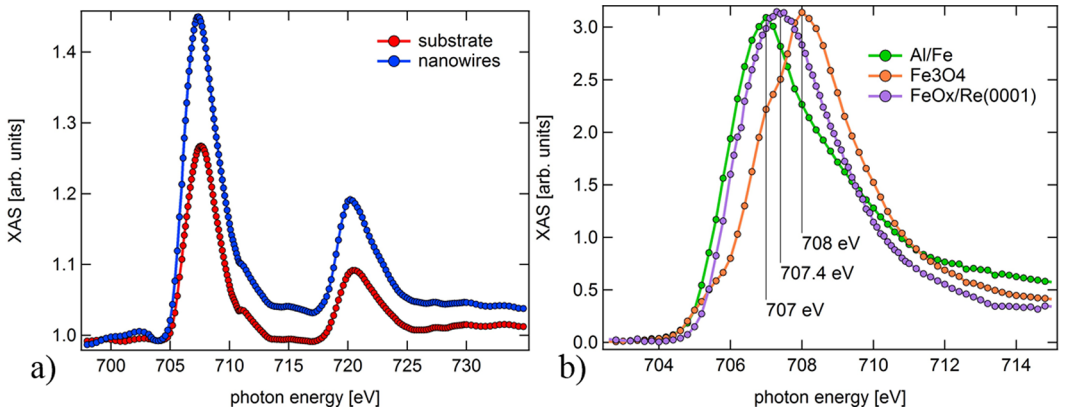


**Figure 4.** XAS at the Fe L absorption edges of (a) nanowires only and the background substrate excluding nanowires for the whole image (with raw signal scaled to 1 pre-edge); (b) a comparison between the nanowires and (Al capped) pure Fe and a bulk $Fe_3O_4$ single crystal all measured on the same PEEM instrument on beamline I06.

dewetting of Fe leaving bare nonmagnetic Re surfaces or a remaining nonmagnetic iron oxide wetting layer. The LEED pattern, however, shows that the FeO(111) structure dominates on the substrate surface indicating that a wetting layer of nonmagnetic FeO(111) remains after dewetting of the excess Fe in the $O_2$ environment.

Having demonstrated that these nanowires are iron rich and single domain magnets we turn now to consider their composition and crystallography. Ferro (and ferri) magnetic iron containing structures could be pure iron which is ferromagnetic, $Fe_3O_4$ magnetite which is ferrimagnetic, or $\gamma$-$Fe_2O_3$ maghemite which is ferromagnetic, whereas other oxides of Fe will not display the observed magnetic signals. The oxygen pressure of $\sim 1 \times 10^{-7}$ mbar is insufficient to fully oxidize iron to $Fe_2O_3$[21] but it is high enough to oxidize pure Fe to FeO or $Fe_3O_4$. We therefore expect magnetite to be the dominant magnetic oxide responsible for the nanowires. To test this hypothesis, we employed XAS in the PEEM on our nanowire samples and also on aluminum-capped pure Fe and $Fe_3O_4$ single crystals. Doing this self-consistently on the same instrument allows direct comparison without having to calibrate photon energies from other sources as the literature contains a wide range of Fe $L_3$ peak absorption energies for these materials.[22] For the nanowire samples we attempt to selectively extract data for the nanowires only and for the substrate uncovered between the dewet nanowires. However, the spatial resolution of the PEEM is comparable to the apparent width of the narrowest nanowires in the LEEM images (~40 nm) and so we expect some small contribution to the nanowire signal from the substrate but not vice versa. Our results are shown in Figure 4 and the XAS response for wires and wetting layer appear to be very similar (also see Movie 5 in SI). The XAS from all the nanowires in the field of view showed a maximal absorption at 707.4 eV, which is the same maxima found for the wetting layer on the substrate. For Fe metal films, the Fe $L_3$ peak was at ~707 eV with a long tail and the single crystal $Fe_3O_4$ peak was at 708.0 eV without a long tail but with a small shoulder at ~707 eV. From this we can see that the nanowire line shape and position differs from a metal considerably confirming that they have oxide character and therefore are not composed of pure Fe. The structure of the wires cannot be determined unequivocally from the XAS measurement.

The very small width and sparseness on the substrate is a problem for further identification by LEEM imaging and PEEM-based spectroscopies and hence we return to STM imaging. The sparseness is still a problem as the imaging field of view is limited (0.8 $\mu$m maximum for our instrument, see SI Figure SI1 for a comparison of imaging scale to island density) but the potential advantage of the high spatial resolution of this microscopy is that it can provide atomic scale structural information. Unfortunately, we also lose the significant ability of LEEM to image dynamically while heating and oxidizing which allows intervention to freeze out the structures once they have been seen to have formed. Figure 5 shows the results of an STM experiment that follows the methodology used in the LEEM/PEEM experiments to form the nanowires. In Figure 5a, two nanowires can be seen running diagonally in the full field of

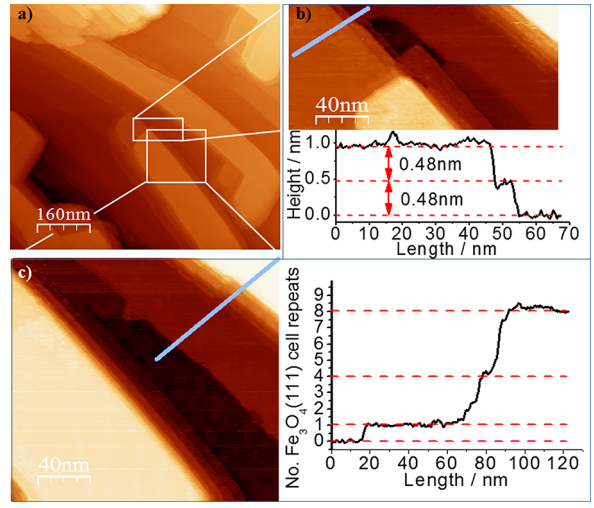


**Figure 5.** STM images ($I_t$ = 1 nA and $V_b$ = 1 V) and cross sectional line profiles of nanowires grown by reactive dewetting of 3 ML iron deposited on a preformed FeO(111) monolayer under $1 \times 10^{-7}$ mbar $O_2$ at ~770 K for 45 min. (a) Maximal field of view image (0.8 $\mu$m) of two elongated wires of ~4 nm height and flat upper facets. Some other residual islands coexist which indicated this is not fully dewet but these also appear with flat upper facets. (b) STM image taken at the rectangle in Figure 6a in which steps are exposed at the edge of the nanowire. A height profile taken along the blue line is shown in the graph with step heights of 0.48 nm. (c) STM image taken in the square of Figure 6a with a line profile across the second nanowire. The profile is scaled in height to the $Fe_3O_4$(111) repeat of 0.48 nm and shows an exact match for integer multiples of this repeat distance.



DOI: 10.1021/acs.nanolett.7b05310
Nano Lett. 2018, 18, 2365−2372

view with other wires crossing opposite corners of the image out of the field of view. All of these structures show an extremely flat upper surface and run across the substrate steps that are just visible in the background (step heights of 0.23 nm corresponding to the Re interlayer spacing) without introducing steps in the wires upper surface. The structure to the top left is attached to a nanowire and appears to also contain multiple flat topped crystallites. We believe this is one of the residual islands apparent in LEEM in areas where dewetting to form nanowires is incomplete. The incomplete nature of the dewetting leads the nanowires to have stepped rather than fully close-packed faceted sides. Close examination of two regions, highlighted by rectangular and square white boxes and shown in detail in Figure 5b,c, identify that the steps all have a common height multiple of 0.48 nm, which corresponds exactly to the interlayer unit cell repeat of magnetite $Fe_3O_4(111)$. The interlayer repeat of FeO(111) is 0.25 nm and for corundum structured $\alpha$-$Fe_2O_3(0001)$ it is 0.29 nm. At these step heights, odd multiples of these steps or even multiples of 0.25 nm that would be close to multiples of 0.48 nm (but distinguishable) are not observed on the wires, therefore we conclude that the wires do not have either of these structures. After imaging, this surface was removed from vacuum and imaged by scanning electron microscopy which confirmed the presence of wires with lengths and widths matching those seen at the maximum field of view of the STM, see SI Figure SI1.

In order to probe the structural relationship between the islands formed on the surface and the substrate, we adopted modified growth protocols to form fully faceted structures that were small enough to image within the STM. The fully faceted long, narrow, and tall nanowires previously discussed become difficult to image by STM as they tend to form double-tipped images very easily which leads to instability (see SI Figure SI2 for examples). Figure 6a–c show STM images and a line profile

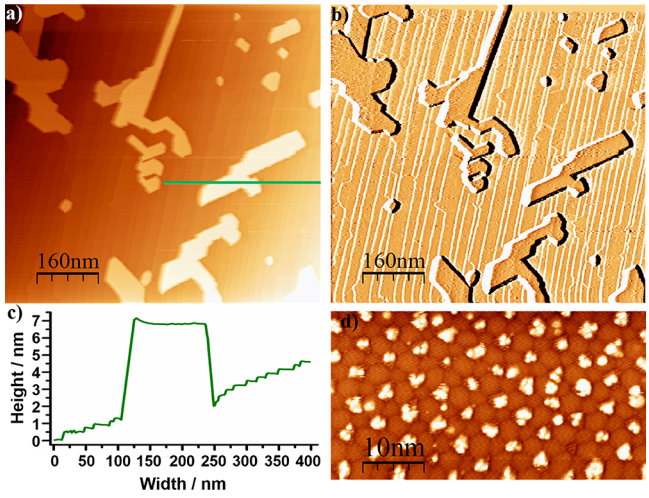


**Figure 6.** (a) STM topographic image ($I_t$ = 0.5 nA and $V_b$ = 1.5 V) of $FeO_x$ islands dewet from a Re(0001) surface. (b) Differential of (a) highlighting terrace steps (and wetting layer grain boundaries) and the flat tops and faceted sides of the crystalline islands. (c) Line profile across substrate and island showing atomic steps on the substrate and atomically smooth upper facet of the island parallel to substrate terraces. (d) High-resolution STM topography ($I_t$ = 0.5 nA and $V_b$ = 1.5 V) from the upper facet of a crystalline nanoisland showing hexagonal array of inclusions as seen in biphase reconstruction of $Fe_3O_4(111)$ single crystals.[24]

across islands and terrace of iron oxide nanostructures dewet from the Re substrate in a single cycle by direct oxidation ($5 \times 10^{-7}$ mbar, 820 K) of 3 ML of Fe (see SI for a Figure SI3 2 ML example). Figure 6a displays the STM topographic image whereas Figure 6b shows the differential image which highlights step and island edges. The images have been tilted such that the substrate terraces are horizontal and this also coincides with the oxide island upper terraces being flat and parallel to the crystallography of substrate surface. In this region of the substrate, there is a high step density and these are readily apparent in the differential image running from top to bottom. The islands do not follow the macroscopic topography, such as predominant step orientation, but are directed by the substrate crystallographic directions. The islands have extended faceted sides along three directions in-plane, one of which coincides with the substrate step structure and is a close packed direction of the substrate, that is, the $\langle 2\bar{1}\bar{1}0\rangle$ family of three equivalent directions, and we therefore conclude the islands align with these directions. In cross section, Figure 6c, the oxide islands can be seen to form as flat mesas in which the top lies parallel to the terraces of the substrate and is not noticeably influenced by the local step density or orientation, in contrast to some dewetting systems.[23] Figure 6d shows the upper facet of a large island (about 11 nm in height, see SI Figure SI4) grown by multiple cycles of deposition and oxidation (+0.5 ML, +0.5 ML, +1 ML, +1 ML, +1 ML each annealed at 820 K in $5 \times 10^{-7}$ mbar $O_2$) on a preformed FeO monolayer to give a total of 5 ML. The low initial deposition steps ensure that islands nucleate very sparsely and subsequent depositions then grow on those centers leading to fewer but larger islands for the same annealing temperatures and pressures. The islands maintain the very flat upper facet morphology seen for all other islands and nanowires grown and although they are no longer elongated along the Re surface crystallographic directions the side facets run in the same directions as seen in Figures 5 and 6a,b. The flatness of the upper terrace can be seen in Figure 6d, where high-resolution STM could be performed on the surface of a large island. This surface is flat but it is also clearly highly structured with small bright clusters decorating a hexagonally reconstructed surface. This morphology is exceptionally similar to the biphase surface structure of $Fe_3O_4(111)$ single crystals as seen in Thornton's work[24] and $Fe_3O_4$ films on Au(111).[25] Between the islands the surface is covered by a FeO wetting layer with a structure very similar to that seen for one monolayer thick films shown in Figure 2 and is responsible for the XAS signal seen between nanowires in Figure 4.

The nanowires dewet from the structure have been demonstrated to generate strong dichroism in XMCD and are therefore ferromagnetic with the imaging showing that these islands each contain a single domain. The STM shows the orientation and phase of the crystalline islands to be related to the substrate crystallography with long axis aligned to close-packed substrate directions. The measured step heights of dewet nanowires are consistent with the formation of $Fe_3O_4(111)$ oriented wires with very flat upper terraces. The STM images on top of mesas of large compact islands indicate they are also $Fe_3O_4(111)$ crystallites and all structures form with $\langle 1\bar{1}0\rangle$ aligned to the substrate $\langle 2\bar{1}\bar{1}0\rangle$. The extended nature of the nanowires, along the $\langle 1\bar{1}0\rangle$ direction with a (111) plane exposed on the surface means that the long side facets are crystallographically inequivalent; one being the (001) plane and the other (110). However, recent DFT calculations of the surface stabilities of magnetite[26] show that the (110) does not



DOI: 10.1021/acs.nanolett.7b05310
Nano Lett. 2018, 18, 2365–2372

appear in the Wulff construction and that $\langle 11\bar{1} \rangle$ facets would in fact bound this edge. {111} surfaces of bulk magnetite are calculated to be slightly less stable than {001} and one might imagine that the nanocrystals growing in heavily stepped regions of the substrate with the {001} forming the larger facets on the downslope with {111} preferred on the upper side facet (and on the mesa surface which is constrained by good epitaxy to the substrate). Currently we cannot directly identify side facet crystallography from our experiments.

One of the primary reasons for dewetting of heteroepitaxial thin films is due to the accumulation of strain energy in the film as it increases in thickness. At a given thickness, this strain energy can no longer be accommodated and either structural defects such as dislocations thread through the film or the film breaks up into thicker islands and a thinner wetting layer. In the former case, the cost is in the dislocation defect energy and the latter increased surface area and energies plus a potential volumetric strain energy contribution due to thicker islands. In the dewetting to islands, some very complex morphologies can arise due to interplays in surface and volume effects.[27] Here we find the dewet oxide islands to be apparently defect free, traversing step edges while maintaining a mesa. However, during the dewetting we have also moved from an Fe/FeO/Re(0001) distinctly layered system to one in which the top layer of Fe is also oxidized. The observed chemical reaction fronts seen here and in recent published studies serve to exemplify the complexities of structural and chemical phase transformations[14b,20] in $FeO_x$ systems, and we expect the kinetics of growth to be complex. However, Tersoff and Tromp have developed an approximate expression that describes shape transformations from compact islands into nanowires based upon the energy of dislocation-free strained islands.[28] The model describes the island growth in which energy is minimized by an island narrowing in width while it extends in length along an orthogonal direction. During this process the island height needs to remain constrained for the model to operate successfully. The model has been shown to describe a variety of systems including Ag nanowires on Si(001), elongated anatase $TiO_2$(001) islands on $SrTiO_3$(001)[27b] and elongated clusters of $CoSi_2$ on Si(001).[29] It is probable that a similar mechanism is responsible for the observations in our studies, in which compact oxide islands elongate and narrow to form extended wires. The height constraint is due to a relatively slow diffusion path to the top of the nanowires compared with a rapid diffusion path to the base. Alternatively one could argue that the growth facet at the end of the $Fe_3O_4$ nanowire is particularly reactive and hence the growth shape is dominated by the kinetics of facet attachment energies rather than equilibrium thermodynamics. However, such a model could be expected to lead to growth directed by the substrate step density, as is seen in Fe growth on Mo(110).[30] We note that at the oxygen chemical potentials employed here that magnetite surfaces are predicted by DFT to oxidize significantly and it is also not clear whether the bulk of the nanowire could truly be described as magnetite due to their very small size in cross-section.[26] It is possible that this shape transformation from compact islands to high aspect ratio wires is accompanied by a change in oxide stoichiometry, possibly forming maghemite which has the magnetite structure but with $Fe^{2+}$ vacancies. Clearly, it would be of interest to search the $P-T$ parameter space experimentally to identify critical island sizes that could transform to functional magnetic nanowires and to be able to simultaneously structurally identify the phase of these very thin wires. Having experimentally identified a new morphology in the heteroepitaxial $FeO_x$ system here it is hoped that further theoretical modeling of surface, interface, and bulk energies may reach sufficient fidelity to enable the prediction of critical island sizes and give rise to better understanding and control of surface-supported nanomaterial growth.

In conclusion, we have shown that high aspect ratio iron oxide nanowires of several microns length and less than 40 nm width can be grown by the reactive dewetting of an iron rich oxide film supported on a rhenium surface. The nanowires are formed in registry with the substrate appearing to be ±5° from a substrate high symmetry direction in large area LEEM images while in STM over short distances on smaller islands these appear to be in epitaxy with the close packed rhenium. The nanowires show distinctive XMCD contrast as a result of each being composed of a single ferro (or ferri) magnetic domain and hence are of potential use in magnetic device and spintronic applications. Step edges at the periphery of the nanowires are consistent with a magnetite structure oriented with the (111) surface facet uppermost. As the FeO wetting layer that accompanies these nanostructures is commonly seen on a variety of other hexagonal substrates it is thought that the growth phenomena is also likely to occur on other substrates with similar lattice constants (Pt, Pd, and so forth). It is further probable that the dewetting follows the Tersoff and Tromp model of shape transformation from compact islands into nanowires based upon the energy of dislocation-free strained islands.

## ■ ASSOCIATED CONTENT

### Supporting Information

The Supporting Information is available free of charge on the ACS Publications website at DOI: 10.1021/acs.nanolett.7b05310.

An expanded experimental description of the methods used and the analysis of XMCD imaging; four sets of images that provide information about the island growth (PDF)

Growth of Fe on the clean Re(0001) surface (AVI)

Formation of nanowires after a reaction front has passed across the Fe on $FeO_x$ surface (AVI)

Formation of nanowires without a surface reaction front traversing the crystal (AVI)

LEED-IV patterns visible prior to nanowire formation (AVI)

Images accompanying the XAS measurements of the nanowires(AVI)

## ■ AUTHOR INFORMATION


### Corresponding Author

*E-mail: r.a.bennett@reading.ac.uk.

### ORCID

Roger A. Bennett: 0000-0001-6266-3510

### Present Address

[‖](C.W.) School of Materials Science and Engineering, Zhejiang University, Hangzhou 310027, China.


### Author Contributions

The manuscript was written through contributions of all authors. All authors have given approval to the final version of the manuscript.



DOI: 10.1021/acs.nanolett.7b05310
Nano Lett. 2018, 18, 2365−2372

### Notes

The authors declare no competing financial interest.

## ■ ACKNOWLEDGMENTS

We would like to thank Diamond Light Source for synchrotron beamtime under proposal SI9309, colleagues at the Diamond synchrotron for supporting the work and also the Royal Society/Wolfson Foundation for facilities refurbishment in Reading. HAE would like to thank the EPSRC for studentship funding. We acknowledge the expertise of Dr Peter Harris of the EMLab at the University of Reading who acquired the SEM images of our nanostructured surface.

## ■ REFERENCES

(1) Zhang, Z.; Satpathy, S. Electron states, magnetism, and the Verwey transition in magnetite. *Phys. Rev. B: Condens. Matter Mater. Phys.* **1991**, *44* (24), 13319−13331.

(2) Parkinson, G. S. Iron oxide surfaces. *Surf. Sci. Rep.* **2016**, *71* (1), 272−365.

(3) Senn, M. S.; Wright, J. P.; Attfield, J. P. Charge order and three-site distortions in the Verwey structure of magnetite. *Nature* **2012**, *481* (7380), 173−176.

(4) Řezníček, R.; Chlan, V.; Štěpánková, H.; Novák, P. Hyperfine field and electronic structure of magnetite below the Verwey transition. *Phys. Rev. B: Condens. Matter Mater. Phys.* **2015**, *91* (12), 125134.

(5) Lee, J.; Kwon, S. G.; Park, J.-G.; Hyeon, T. Size Dependence of Metal−Insulator Transition in Stoichiometric $Fe_3O_4$ Nanocrystals. *Nano Lett.* **2015**, *15* (7), 4337−4342.

(6) Parkinson, G. S.; Diebold, U.; Tang, J.; Malkinski, L. *Tailoring the Interface Properties of Magnetite for Spintronics, Advanced Magnetic Materials*; Malkinski, L., Ed.; InTech: 2012.

(7) Liao, Z.-M.; Li, Y.-D.; Xu, J.; Zhang, J.-M.; Xia, K.; Yu, D.-P. Spin-Filter Effect in Magnetite Nanowire. *Nano Lett.* **2006**, *6* (6), 1087−1091.

(8) Yun, J.-G.; Lee, Y.-M.; Lee, W.-J.; Kim, C.-S.; Yoon, S.-G. Selective growth of pure magnetite thin films and/or nanowires grown in situ at a low temperature by pulsed laser deposition. *J. Mater. Chem. C* **2013**, *1* (10), 1977−1982.

(9) Takahashi, R.; Misumi, H.; Yamamoto, T.; Lippmaa, M. Spontaneous Growth of Strain-Free Magnetite Nanocrystals via Temperature-Driven Dewetting. *Cryst. Growth Des.* **2014**, *14* (3), 1264−1271.

(10) Tauster, S. J.; Fung, S. C.; Garten, R. L. Strong metal-support interactions. Group 8 noble metals supported on titanium dioxide. *J. Am. Chem. Soc.* **1978**, *100* (1), 170−175.

(11) Braunschweig, E. J.; Logan, A. D.; Datye, A. K.; Smith, D. J. Reversibility of strong metal-support interactions on $RhTiO_2$. *J. Catal.* **1989**, *118* (1), 227−237.

(12) Datye, A. K.; Kalakkad, D. S.; Yao, M. H.; Smith, D. J. Comparison of Metal-Support Interactions in $Pt/TiO_2$ and $Pt/CeO_2$. *J. Catal.* **1995**, *155* (1), 148−153.

(13) (a) Willinger, M. G.; Zhang, W.; Bondarchuk, O.; Shaikhutdinov, S.; Freund, H.-J.; Schlögl, R. A Case of Strong Metal−Support Interactions: Combining Advanced Microscopy and Model Systems to Elucidate the Atomic Structure of Interfaces. *Angew. Chem., Int. Ed.* **2014**, *53* (23), 5998−6001. (b) Majzik, Z.; Balázs, N.; Berkó, A. Ordered SMSI Decoration Layer on Rh Nanoparticles Grown on $TiO_2$(110) Surface. *J. Phys. Chem. C* **2011**, *115* (19), 9535−9544. (c) Bennett, R. A.; Pang, C. L.; Perkins, N.; Smith, R. D.; Morrall, P.; Kvon, R. I.; Bowker, M. Surface Structures in the SMSI State; Pd on (1 × 2) Reconstructed $TiO_2$(110). *J. Phys. Chem. B* **2002**, *106* (18), 4688−4696. (d) Silly, F.; Castell, M. R. Encapsulated Pd Nanocrystals Supported by Nanoline-Structured $SrTiO_3$(001). *J. Phys. Chem. B* **2005**, *109* (25), 12316−12319.

(14) (a) Qiu, H.; Staemmler, V.; Kuhlenbeck, H.; Bauer, E.; Freund, H.-J. Weak thermal reduction of biphase $Fe_2O_3$(0001) films grown on Pt(111): Sub-surface $Fe^{2+}$ formation. *Surf. Sci.* **2015**, *641*, 30−36. (b) Genuzio, F.; Sala, A.; Schmidt, T.; Menzel, D.; Freund, H.-J. Interconversion of $\alpha$-$Fe_2O_3$ and $Fe_3O_4$ Thin Films: Mechanisms, Morphology, and Evidence for Unexpected Substrate Participation. *J. Phys. Chem. C* **2014**, *118* (50), 29068−29076. (c) Ketteler, G.; Ranke, W. Self-assembled periodic $Fe_3O_4$ nanostructures in ultrathin FeO(111) films on Ru(0001). *Phys. Rev. B: Condens. Matter Mater. Phys.* **2002**, *66* (3), 033405. (d) Santos, B.; Loginova, E.; Mascaraque, A.; Schmid, A. K.; McCarty, K. F.; de la Figuera, J. Structure and magnetism in ultrathin iron oxides characterized by low energy electron microscopy. *J. Phys.: Condens. Matter* **2009**, *21* (31), 314011.

(15) Etman, H. A.; Zheleva, Z. V.; Held, G.; Bennett, R. A. Epitaxial Growth of Ultrathin Palladium Films on Re{0001}. *J. Phys. Chem. C* **2011**, *115* (10), 4191−4199.

(16) Horcas, I.; Fernández, R.; Gómez-Rodríguez, J. M.; Colchero, J.; Gómez-Herrero, J.; Baro, A. M. WSXM: A software for scanning probe microscopy and a tool for nanotechnology. *Rev. Sci. Instrum.* **2007**, *78* (1), 013705.

(17) Ritter, M.; Ranke, W.; Weiss, W. Growth and structure of ultrathin FeO films on Pt(111) studied by STM and LEED. *Phys. Rev. B: Condens. Matter Mater. Phys.* **1998**, *57* (12), 7240−7251.

(18) Merte, L. R.; Grabow, L. C.; Peng, G.; Knudsen, J.; Zeuthen, H.; Kudernatsch, W.; Porsgaard, S.; Lægsgaard, E.; Mavrikakis, M.; Besenbacher, F. Tip-Dependent Scanning Tunneling Microscopy Imaging of Ultrathin FeO Films on Pt(111). *J. Phys. Chem. C* **2011**, *115* (5), 2089−2099.

(19) Berdunov, N.; Mariotto, G.; Murphy, S.; Balakrishnan, K.; Shvets, I. V. Self-assembly of iron nanoclusters on the $Fe_3O_4$(111) superstructured surface. *Phys. Rev. B: Condens. Matter Mater. Phys.* **2005**, *71* (11), 113406.

(20) Genuzio, F.; Sala, A.; Schmidt, T.; Menzel, D.; Freund, H. J. Phase transformations in thin iron oxide films: Spectromicroscopic study of velocity and shape of the reaction fronts. *Surf. Sci.* **2016**, *648*, 177−187.

(21) Monti, M.; Santos, B.; Mascaraque, A.; Rodríguez de la Fuente, O.; Niño, M. A.; Menteş, T. O.; Locatelli, A.; McCarty, K. F.; Marco, J. F.; de la Figuera, J. Oxidation Pathways in Bicomponent Ultrathin Iron Oxide Films. *J. Phys. Chem. C* **2012**, *116* (21), 11539−11547.

(22) Regan, T. J.; Ohldag, H.; Stamm, C.; Nolting, F.; Luning, J.; Stohr, J.; White, R. L. Chemical effects at metal/oxide interfaces studied by x-ray-absorption spectroscopy. *Phys. Rev. B: Condens. Matter Mater. Phys.* **2001**, *64* (21), 214422.

(23) Ling, W. L.; Giessel, T.; Thürmer, K.; Hwang, R. Q.; Bartelt, N. C.; McCarty, K. F. Crucial role of substrate steps in de-wetting of crystalline thin films. *Surf. Sci.* **2004**, *570* (3), L297−L303.

(24) Condon, N. G.; Leibsle, F. M.; Parker, T.; Lennie, A. R.; Vaughan, D. J.; Thornton, G. Biphase ordering on $Fe_3O_4$(111). *Phys. Rev. B: Condens. Matter Mater. Phys.* **1997**, *55* (23), 15885−15894.

(25) Deng, X.; Lee, J.; Matranga, C. Preparation and characterization of $Fe_3O_4$(111) nanoparticles and thin films on Au(111). *Surf. Sci.* **2010**, *604* (7), 627−632.

(26) Santos-Carballal, D.; Roldan, A.; Grau-Crespo, R.; de Leeuw, N. H. A DFT study of the structures, stabilities and redox behaviour of the major surfaces of magnetite $Fe_3O_4$. *Phys. Chem. Chem. Phys.* **2014**, *16* (39), 21082−21097.

(27) (a) Bennett, R. A.; Mulley, J. S.; Etman, H. A.; Sparkes, A.; Eralp, T.; Held, G.; Cavill, S. A.; Dhesi, S. S. Chromium nanostructures formed by dewetting of heteroepitaxial films on W(100). *Phys. Rev. B: Condens. Matter Mater. Phys.* **2012**, *86* (4), 045454. (b) Marshall, M. S. J.; Castell, M. R. Shape Transitions of Epitaxial Islands during Strained Layer Growth: Anatase $TiO_2$(001) on $SrTiO_3$(001). *Phys. Rev. Lett.* **2009**, *102* (14), 146102.

(28) Tersoff, J.; Tromp, R. M. Shape transition in growth of strained islands: Spontaneous formation of quantum wires. *Phys. Rev. Lett.* **1993**, *70* (18), 2782−2785.

(29) Brongersma, S. H.; Castell, M. R.; Perovic, D. D.; Zinke-Allmang, M. Stress-Induced Shape Transition of $CoSi_2$ Clusters on Si(100). *Phys. Rev. Lett.* **1998**, *80* (17), 3795−3798.



DOI: 10.1021/acs.nanolett.7b05310
*Nano Lett.* 2018, 18, 2365−2372

(30) Shvets, I. V.; Murphy, S.; Kalinin, V. Nanowedge island formation on Mo(110). *Surf. Sci.* **2007**, *601* (15), 3169−3178.



DOI: 10.1021/acs.nanolett.7b05310
*Nano Lett.* 2018, 18, 2365−2372